Progress In Electromagnetics Research, Vol. 125, 185–202, 2012

RADIAL FORCE CHARACTERISTIC ASSESSMENT IN A NOVEL TWO-PHASE DUAL LAYER SRG USING FEM

H. Torkaman[1,*] and E. Afjei[2]

[1]Young Researchers Club, South Tehran Branch, Islamic Azad University, Tehran, Iran

[2]Department of Electrical Engineering, Shahid Beheshti University, G.C., Tehran, Iran

Abstract—This paper investigates the radial force characteristics of a novel two-phase dual layer switched reluctance generator. The proposed generator consists of two magnetically dependent stator and rotor layers, where each stator set includes four salient poles with windings wrapped around them while, the rotor comprises of two salient poles. In this paper, the radial and tangential force components and their trends in healthy condition under different load levels are assessed with the respect to critical rotor positions. One of the most important problems seen in the industrial applications of generators which have concerned users is the rotor eccentricity which may conclude the unbalanced distribution of flux linkage as well as acoustic noise and vibration due to the radial forces produced during the rotation of machine's rotor. In this regard, in this paper, it is attempted to obtain and evaluate the radial force components resulted from different degrees of eccentricity faults.

1. INTRODUCTION

Switched Reluctance Motor and Generators are attractive solutions for worldwide increasing demand of electrical energy. They have low cost, are fault tolerant with a rugged structure, and operate with high efficiency over a wide speed range. Merits of using SRG have been proved for some applications like starter/generator for gas turbine of aircrafts, windmill generator and as an alternator for automotive applications [1–4].

Received 4 January 2012, Accepted 13 February 2012, Scheduled 26 February 2012

* Corresponding author: Hossein Torkaman (H_torkaman@sbu.ac.ir).

SRMs is based on tendency of the polarized rotor pole in achieving full alignment position with the excited stator pole which provokes whirling mode of the motor. Tangential and radial forces are two components of this magnetism force. The TF transforms into the rotational torque [5–7]. Generally, in balanced motor operation, the total of RF is zero at ideal mode. However, faulty operation caused by asymmetric structure, mechanical faults or environmental motivations gives unbalanced RFs. These forces are undesirable and they result in motor vibrations. For instance, unbalanced external load or eccentricity fault leads to form asymmetrical air gap and then produces an acoustic noise and UMP, due to formed RF [8, 9].

In [8], a method has been implemented for RF and torque control for rotating and levitating 12/8 SRM. In this scheme, the RF and motor average torque are independently controlled using hybrid excitations in main windings and levitation windings. In [10] and [11], a new control strategy was presented, that the shaft RF and the torque of a SRM are controlled separately by selection the proper pole current in the energized phase. In [12], to control a 12/8 SRM, a RF and torque decoupling control pattern has been proposed with a main and an auxiliary windings in each pole. In [13] a method based on a thin cylinder approximation of the stator has been presented, to determine the harmonic content of stator vibrations and acoustic noise resulting from RF excitations in SRM. The reduction of vibration and acoustic noise in SRM have been discussed in [14]. The vibration has been determined by two factors, the RF excitation and the structure borne transfer function.

Therefore, it is necessary to detect mechanical fault such as eccentricity at an early time as well as RF analysis in the motor to avoid disastrous failures [15, 16]. Different studies have investigated and analyzed the RF of SRMs and proposed number of methods in order to control and compensate it over the last years [17–19].

In the previous works [3, 5, 20], the authors have presented different structures of the SRM/SRG and analyzed them under healthy conditions. Then in [21, 22] and [6, 23], the SE and DE in the SRM and SRG are assessed, respectively. Moreover, the ME, misalignment and angular misalignment in this motor are appraised in [4, 24] and [1], respectively. Afterward, the intervals for different modes of motor operation (normal and faulty) are calculated by a hybrid Genetic method in [2] and utilizing a nonlinear torque function in [25].

In this paper, the RF characteristic is assessed in a novel two-phase DLSRG to investigate the generator operation mode and to avoid ruinous failures. This paper is organized as follows; the proposed two-phase DLSRG structure is described in Section 2. The RF

characteristic of the SRM is introduced in Section 3. In Section 4 the principle of flux density, RF changes as well as effects of excited current are investigated and analyzed in Section 5. Finally, the concluding remarks are illustrated in Section 6.

2. THE DLSRG CONFIGURATION DESCRIPTION

The proposed novel DLSRG consists of two magnetically dependent stator and rotor layers, where each stator set includes four salient poles with windings wrapped around them while, the rotor comprises of two salient poles. Every stator and rotor pole arcs are 45°. The two layers are exactly symmetrical with respect to a plane perpendicular to the middle of the generator shaft. This is a two phase generator; therefore, each layer consists of four stator poles and two rotor poles, respectively.

In the generating mode the coil windings in each layer are such that the stator poles gain either North or South Pole configuration. In other words, each layer consists of a four by two reluctance motor configuration sharing common shaft operating in sequence. There is a stationary reel, which has the field coils wrapped around it and is placed between the two-stator layers. This reel has a rotating cylindrical core, which guides the magnetic field. In order to get a better illustration of the proposed DLSRG configuration, the complete simulated assembly and the built prototype are presented in Figs. 1(a) and (b), respectively.

The magnetic flux produced by the coils travels through the guide and shaft to the rotor and then to the stator poles, and finally closes itself through the generator housing. Therefore, one set of rotor poles is magnetically north and the other set is magnetically south. There are two stators and rotors sections placed on both sides of the field coil

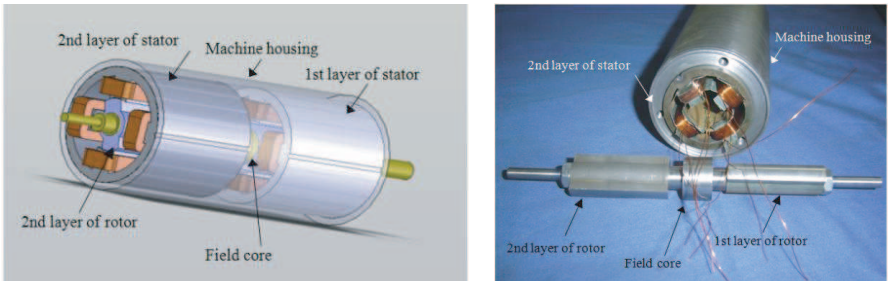

(a) (b)

Figure 1. The complete assembly of DLSRG: (a) Simulated generator. (b) Real scheme of the prototype.

assembly which has the rotor shaft as its main core and two front/end caps plus the generator housing. A set of photo interrupters are also place in the back of the generator for the detection of rotor position. The proposed generators dimensions are listed in Table 1.

In order to analyze the real performance of the proposed DLSRG, the speed of this generator must be adjusted to study its performance. Therefore, the speed of this generator has been determined equal to 2225 rpm until the performance and output voltage of this proposed generator can be compared with the output voltage and the real performance of the proposed DLSRG. In order to adjust the speed of this generator and keeping it constant, a conventional SRM has been utilized as prime mover.

Table 1. The DLSRGs' specifications.

Parameter	Value
Stator core outer diameter	52 mm
Stator arc	45 deg
Air gap	0.25 mm
Rotor core outer diameter	25 mm
Rotor shaft diameter	7 mm
Rotor arc	45 deg
Number of turns per pole	250
Stack length	280 mm
Number of turns in field coil	250

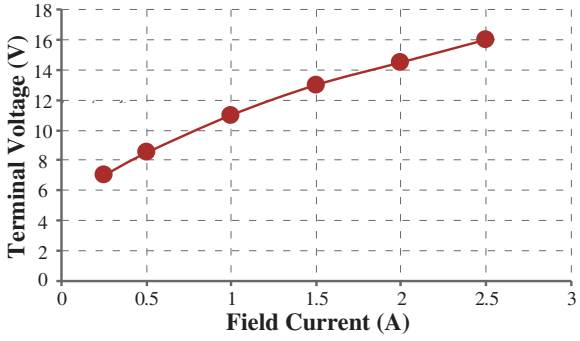

Figure 2. Generator terminal voltage vs. field current.

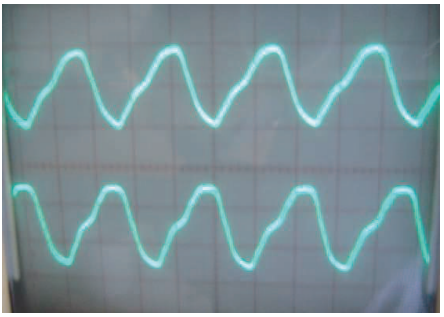

Figure 3. The output voltages for two consecutive phases (5 V/div).

The generated voltage in each pole of the proposed generators can be calculated by Equation (1);

$$e_{\text{ind}} = \frac{\partial \lambda}{\partial t} = \frac{\partial (Li)}{\partial t} = L\frac{\partial i}{\partial t} + i\frac{\partial L}{\partial t} \tag{1}$$

Since current, i in each pole is kept constant so Equation (1) can be rewritten as:

$$e_{\text{ind}} = i\frac{\partial L}{\partial \theta}\omega = N\frac{\partial \varphi}{\partial \theta}\omega \tag{2}$$

The ω is generator angular speed in *rad/sec*, λ shows the flux linkage acquired by multiplying each coil's number of turns by the magnetic flux of that coil, θ shows the rotor position in *rad* and L stands for the inductance of each phase.

Based on mentioned equation, in laboratory, the produced voltage in proposed generator is monitored. The speed of the motor kept constant for various field currents, the resulting terminal voltage is shown in Fig. 2.

In this figure, curve fitting (power) has been used for better presentation of the data points.

The output voltage for two consecutive phases of this generator is shown in Fig. 3. It is worth noting that each unit on oscilloscope's sheet is equal to 5 V/div.

The phase shift is clearly shown in Fig. 3. The voltages have harmonics which are due to the shape of the stator and rotor poles as well as saturation inside them.

3. RADIAL FORCE CHARACTERISTICS

A precise model is needed for the physical motor simulation to incorporate the essential dynamics of the motor [26–29]. The Finite

Element Method can be one of the best choices for providing realistic and precise model [30–34]. The 3D-FEM has been used in this investigation. To present the operation of the motor and to determine the static torque at different positions of the rotor, the field solutions are obtained for different rotor positions when each phase is excited. The 3D solution considers all the fringing and leakage field components, which some of them are ignored in two dimensional models. In this method, electric vector potential (T) has been utilized for solving the magnetic field problems. This method is based on the variational energy minimization technique to solve for the electric vector potential. In this method, electric vector potential is defined and used. This method is known as $T-\Omega$ formulation where T defined by;

$$J = \nabla \times T \tag{3}$$

From Maxwell's equation;

$$\nabla \times H = J = \nabla \times T \tag{4}$$

Then

$$\nabla \times (H - T) = 0 \tag{5}$$

Since the vector $(H - T)$ can be expressed as the gradient of a scalar, i.e.,

$$H = T - \nabla\Omega \tag{6}$$

where Ω is a magnetic scalar potential.

And, since

$$\nabla \times E = -\frac{\partial B}{\partial t} \tag{7}$$

Then,

$$\begin{aligned} \nabla \times E &= \nabla \times \left[\left(\frac{1}{\sigma}\right) \nabla \times T\right] = -\frac{\partial B}{\partial t} \\ &= -\mu_0\mu_r \left(\frac{\partial}{\partial t}\right)(T - \nabla\Omega) = -\mu_0\mu_r \left(\left(\frac{\partial T}{\partial t}\right) - \nabla\left(\frac{\partial \Omega}{\partial t}\right)\right) \end{aligned} \tag{8}$$

which finally reduces to the following two scalar equations

$$\nabla^2 T - \mu\sigma\left(\frac{\partial T}{\partial t}\right) = -\mu\sigma\nabla\left(\frac{\partial \Omega}{\partial t}\right) \tag{9}$$

And

$$\nabla^2\Omega = 0 \tag{10}$$

When a three dimensional magnetic field problem is solved by magnetic vector potential (A), the need to solve for all the

three components of A arises, whereas using the $T - \Omega$ method, T can be simplified to produce the necessary solutions with only two components.

In this study, the usual assumptions such as the magnetic field outside the motor periphery is considered zero. For convenience, the position, when a stator pole is opposite a rotor pole such that the reluctance of the motor magnetic structure is minimum, is defined as the aligned position. This location is assumed to be 90 degrees for the rotor position in the motors performance plots. The unaligned position (zero degree) is defined as that when the rotor pole is in opposite the stator slot such that the reluctance of the motor magnetic structure is at its maximum. In the analysis, the rotor moves from unaligned to aligned positions.

When a specific type of fault like eccentricity fault occurs during the motion of the SRG, some of the electromagnetic characteristics of the studied machine are affected, and the performance of the machine is disturbed. One of the most important electromagnetic traits of the machine which can be remarked relating to this issue is the RF.

In order to analyze and introduce the RF characteristic, its mathematical formulation and the schematic depiction must be illustrated firstly. The calculations of the RFs are based on Maxwell Stress Tensor. The closed-form formulas for RF and TF can be exposed as follows, based on Maxwell Stress Tensor;

$$f_n = \frac{1}{2\mu_0}\left(B_n^2 - B_t^2\right) \tag{11}$$

$$f_t = \frac{1}{2\mu_0} B_n B_t \tag{12}$$

where f_n, f_t are the produced radial and tangential forces, respectively. The B_n, B_t and μ_0 are the normal component, the tangential component of the flux densities, and absolute permeability, respectively.

It can be concluded that B_n and B_t should be equal in healthy generator and ideal condition, which results in zero value for their differences as well as RF. This ideal condition is not appeared in all machines, because of their asymmetric structure, assembly errors and load fluctuations. Therefore, it is noticeable that the maintaining RF in minimum value is essential to avoid noise and vibration producing.

Briefly note that the RF is a force seen during the motion of machine and aligned to the radius of the circle in which rotor passes. In order to be more familiar with the real depiction of this force and its elements, Fig. 4 is presented.

According to Fig. 4, it is quite clear that the total radial force is derived from the horizontal radial force, which is aligned on the X

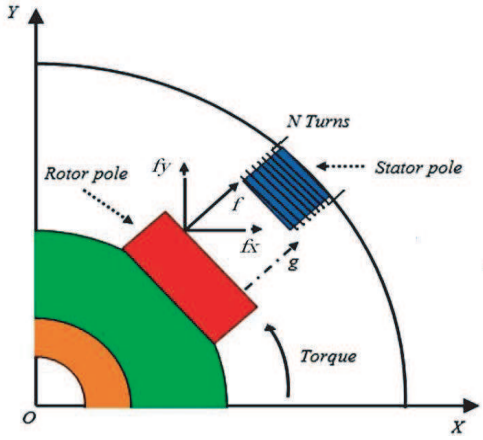

Figure 4. The depiction of the main elements, parameters and orientation of radial force in the studied SRG.

axis and the vertical radial force which is aligned on the Y axis, thus via using these two elements the magnitude of total radial force is presented by

$$f = \sqrt{f_x^2 + f_y^2} \tag{13}$$

After this description, the next section will focus on the effects of static eccentricity fault on the variations of each horizontal, vertical and finally total radial forces separately. It will be seen that increment of faults occuring during the generator's performance enhances the amount of RFs and may produce eventual vibrations and consequently the acoustic noise.

4. ASSESSMENT OF THE RADIAL FORCE CHARACTERISTIC

This section is an attempt to study the radial force profile in DLSRG under different loads as well as evaluate effects of the different degrees of static eccentricity fault on the RF. In addition, in each analysis the healthy generator profiles are compared to the faulty generator profiles.

For the first step of this analysis, the variations of radial field stress versus contour position under different loads are calculated for DLSRG. These profiles are shown in Fig. 5, for half aligned and fully aligned rotor positions.

As shown in Fig. 5, the amplitude of radial field stress profile increases nonlinearly. In fact, as the current enhances, the amplitude increases more slowly due to the saturation effect.

As the rotor leaves the unaligned position toward half aligned position, the overlap between rotor and stator poles has begun. Hence, effects of local saturation are visible in Fig. 5(a). As it is shown, the radial field stress is increased with the ratio of 4, when the exciting current has increased from 2A to 6A.

As rotor leaves the half aligned position toward fully aligned position, the maximum value of radial field stress decreases in higher currents, but the width of the region within which the radial component exists increases. It means that the average radial force has its own maximum value at fully aligned position as it was expected.

In the next step of this analysis, the variations of tangential field stress versus contour position under different loads are calculated for DLSRG. These profiles are revealed in Fig. 6, for half aligned and fully aligned rotor positions.

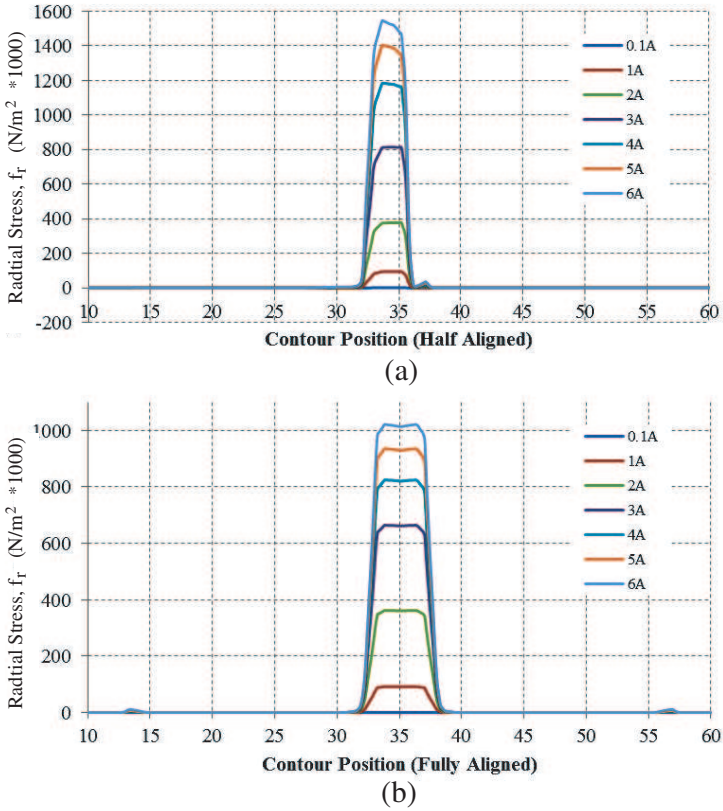

Figure 5. Radial field stress versus contour position under different loads in (a) half aligned, and (b) fully aligned rotor positions.

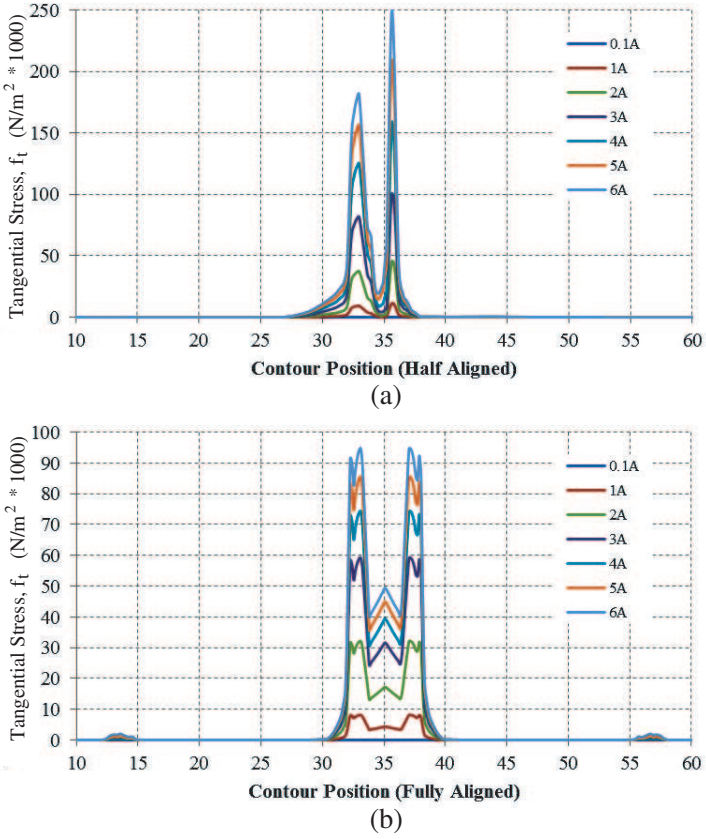

Figure 6. Tangential field stress versus contour position under different loads in; (a) half aligned, and (b) fully aligned rotor positions.

As shown in Fig. 6, the tangential field stresses are increased when the load level is increased. These additive trends in linear operation are higher than those are obtained in nonlinear operation region of the generator, which is due to the effects of local saturation at rotor and stator poles in nonlinear region. This phenomena point out the local maximum value in B_t.

When the rotor pole moves to fully aligned position, the maximum value of tangential field stress decreases dramatically, but the width of the region within which the tangential component exists increases. It is important to note that a largely normal force exists at aligned rotor position that is substantially stronger than tangential component.

Based on the mentioned theory in Section 3, in this part of the study it has been attempted to analysis the effects of the different

percentages of static eccentricity faults equal to 10%, 20%, 40% and 60% on the radial forces components including f_x, f_y and total RF of the DLSRG. In this regard, the static eccentricity is considered. This type of fault occurs when the rotational axis of the rotor is identical to its symmetrical axis but has been displaced from the stator symmetrical axis. Although the air gap distribution around the rotor is not uniform, it is time-independent.

The variations of horizontal (f_x) and vertical (f_y) radial forces in healthy as well as faulty DLSRG are depicted by Figs. 7(a) and (b), respectively. It is worth noting that f_z is the axial force seen

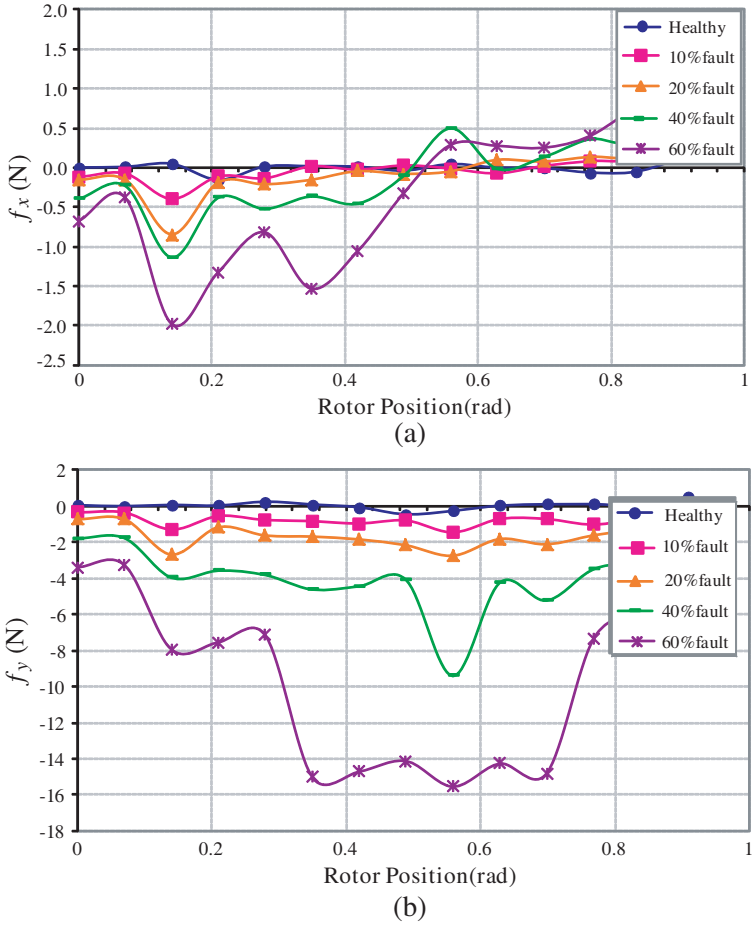

Figure 7. Radial force variations along two axes in healthy and faulty conditions. (a) Along x axis. (b) Along y axis.

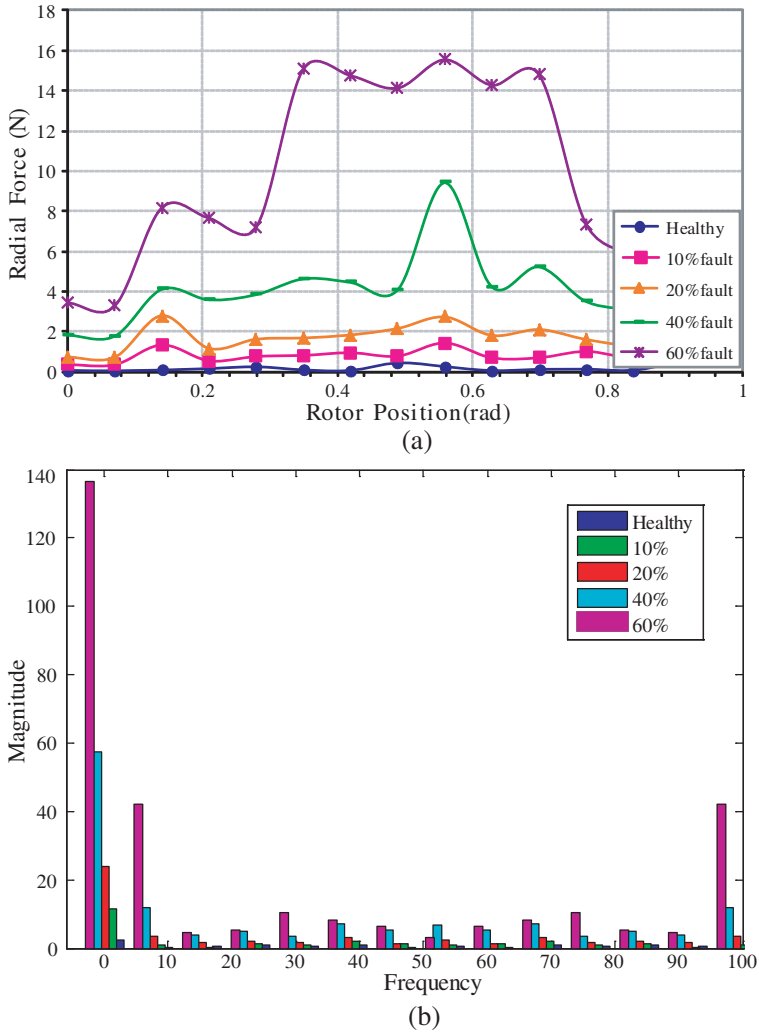

Figure 8. The radial forces in healthy generator and eccentric generator under different degrees of fault. (a) Produced RF. (b) Frequency spectrum.

in the direction of the z axis along with generator length. Since the eccentricity fault has occurred only along the y axis, a very low level of radial force variations is sensed in z axis direction in faulty conditions, and it is not considered in this study.

According to Fig. 7, it is illustrated that the variations of all radial force components, including f_x, f_y, are lower than 0.2 and almost equal to zero, which demonstrates the suitable status of DLSRG's

performance in healthy conditions. This discrepancy is seen in real conditions also since the perfect physical structure for a machine is not obtained in real applications.

It is seen that when the level of fault is increased from 10% up to 60% eccentricities, the RF component toward the y axis is associated with higher amplitude than those obtained in x axis. This phenomenon points to the direction of fault that occurs along y axis.

With respect to Equation (13) and according to the figure above, Fig. 8(a) show the variations of total produced RFs under 10%, 20%, 40% and 60% static eccentricity faults in DLSRG. Furthermore, the FFT has been applied to the waveform of resulted RF when different eccentricities occur in the machine and is shown in Fig. 8(b). The results show a sensitivity of the motor harmonics to changes within the radial force caused by the fault.

According to Fig. 8(a), it is realized that the amplitude of RF is almost zero in healthy motor. Besides, when the degree of eccentricity fault is increased from 10% to 20%, 40% and 60% the maximum radial force has 1.6, 6.3 and 10.3 times higher value than 10% fault. As understood from these results, the proposed DLSRG is robust in front of eccentricity fault up to 20%, which makes it suitable generator for different application under different levels of load and able to use in very harsh environment.

On the other side, the obtained incremental steps show a beneficial pattern for detection the percentage of static eccentricity in this type of generator.

As illustrated in Fig. 8(b), it is realized that when an eccentricity fault occurs, the harmonic components are increased compared with healthy conditions. For instance, when the 60%, 40%, 20% and 10% of eccentricity faults occur, the amplitudes of fundamental component are increased with the ratios of 53, 22, 9 and 4, with respect to the fundamental components in healthy condition.

As mentioned in previous sections, the RF produced due to the eccentricity fault may be very destructive and cause harsh effects on the control, rotor position and performance of DLSRG. Therefore, some methods must be devised to control or compensate the produced forces. In this regard, several studies proposed the search coils which are placed on the stator poles to produce an additional force on the opposite of radial force direction for compensating it. On the other side, kinds of transducers are placed on the generator to investigate these forces and their amplitudes and then control their values with control unit. As mentioned before, the proposed DLSRG is robust in front of eccentricity fault up to 20%. Furthermore, the special structure of this generator leads to avoid adding an additional search coil in

the stator poles. This generator consists of two layers of the stator; therefore, when the fault occurs in one layer, by a proper control in the stator phases of another layer, the fault can be compensated.

5. CONCLUSION

In this paper, a DLSRG is introduced firstly and analyzed in terms of its RFs under different conditions. In this regard, the radial and tangential force stresses are evaluated under different load levels. Then, the generator is placed in the presence of an eccentric condition. As the rotor leaves the unaligned position toward half aligned position, the overlap between rotor and stator poles begins, and effects of local saturation are noticeable. As shown, the radial field stress is increased with the factor of 4, when the exciting current has increased from 2A to 6A. The variation of force components such as horizontal, vertical and total forces is assessed under different degrees of eccentricity. It is illustrated that when the severity of eccentricity is increased, the RF amplitude of the generator is increased, which is considerable in the linear generator operation. As revealed in results, when the degree of eccentricity fault is increased from 10% to 20%, 40% and 60% the maximum RF has 1.6, 6.3 and 10.3 times higher values than 10% fault. Moreover, their FFTs are increased with the ratio of 4, 9, 22 and 53. This gauge could help user to detect the occurrence of fault and may eradicate different problems related to the eccentricity faults. Moreover, it is stated that the proposed DLSRG is robust in front of eccentricity fault because of its special structure.

APPENDIX A. NOMENCLATURE

DE	*Dynamic Eccentricity*
DLSRG	*Dual Layer Switched Reluctance Generator*
FEM	*Finite Element Method*
FFT	*Fast Fourier Transform*
ME	*Mixed Eccentricity*
RF	*Radial Force*
SE	*Static Eccentricity*

SRG *Switched Reluctance Generator*
SRM *Switched Reluctance Motor*
TF *Tangential Force*
UMP *Unbalanced Magnetic Pull*

REFERENCES

1. Torkaman, H. and E. Afjei, "FEM analysis of angular misalignment fault in SRM magnetostatic characteristics," *Progress In Electromagnetics Research*, Vol. 104, 31–48, 2010.
2. Torkaman, H. and E. Afjei, "Hybrid of freedom for radial airgap length in SRM under normal and faulty conditions based on magnetostatic model," *Progress In Electromagnetics Research*, Vol. 100, 37–54, 2010.
3. Torkaman, H., E. Afjei, and M. S. Toulabi, "New double-layer-per-phase isolated switched reluctance motor: Concept, numerical analysis, and experimental confirmation," *IEEE Transactions on Industrial Electronics*, Vol. 59, No. 2, 830–838, 2012.
4. Torkaman, H., E. Afjei, R. Ravaud, et al., "Misalignment fault analysis and diagnosis in switched reluctance motor," *International Journal of Applied Electromagnetics and Mechanics*, Vol. 36, No. 3, 253–265, 2011.
5. Afjei, E. and H. Torkaman, "Comparison of two types of dual layer generator in field assisted mode utilizing 3D-FEM and experimental verification," *Progress In Electromagnetics Research B*, Vol. 23, 293–309, 2010.
6. Torkaman, H. and E. Afjei, "Magnetio static field analysis regarding the effects of dynamic eccentricity in switched reluctance motor," *Progress In Electromagnetics Research M*, Vol. 8, 163–180, 2009.
7. Wen, D. and L. Deliang, "Modeling of a 6/4 switched reluctance motor using adaptive neural fuzzy inference system," *IEEE Transactions on Magnetics*, Vol. 44, No. 7, 1796–1804, 2008.
8. Cao, X., Z. Deng, G. Yang, et al., "Independent control of average torque and radial force in bearingless switched-reluctance motors with hybrid excitations," *IEEE Transactions on Power Electronics*, Vol. 24, No. 5, 1376–1385, 2009.
9. Morrison, C. R., M. W. Siebert, E. J. Ho, et al., "Electromagnetic forces in a hybrid magnetic-bearing switched-reluctance motor," *IEEE Transactions on Magnetics,* Vol. 44, No. 12, 4626–4638, 2008.

10. Lin, F. C. and S. M. Yang, "An approach to producing controlled radial force in a switched reluctance motor," *IEEE Transactions on Industrial Electronics*, Vol. 55, No. 4, 2137–2146, 2007.
11. Lin, F. C. and S. M. Yang, "Instantaneous shaft radial force control with sinusoidal excitations for switched reluctance motors," *IEEE Transactions on Energy Conversion*, Vol. 22, No. 3, 629–636, 2007.
12. Takemoto, M., A. Chiba, H. Suzuki, et al., "Radial force and torque of a bearingless switched reluctance motor operating in a region of magnetic saturation," *IEEE Transactions on Industry Applications*, Vol. 40, No. 1, 103–112, 2004.
13. Fiedler, J. O., K. A. Kasper, and R. W. De Doncker, "Calculation of the acoustic noise spectrum of SRM using modal superposition," *IEEE Transactions on Industrial Electronics*, Vol. 57, No. 9, 2939–2945, 2010.
14. Li, J. and Y. Cho, "Investigation into reduction of vibration and acoustic noise in switched reluctance motors in radial force excitation and frame transfer function aspects," *IEEE Transactions on Magnetics*, Vol. 45, No. 10, 4664–4667, 2009.
15. Dorrell, D. G., M. Popescu, and D. M. Ionel, "Unbalanced magnetic pull due to asymmetry and low-level static rotor eccentricity in fractional-slot brushless permanent-magnet motors with surface-magnet and consequent-pole rotors," *IEEE Transactions on Magnetics*, Vol. 46, No. 7, 2675–2685, 2010.
16. Wang, L., R. W. Cheung, Z. Ma, et al., "Finite-element analysis of unbalanced magnetic pull in a large hydro-generator under practical operations," *IEEE Transactions on Magnetics*, Vol. 44, No. 6, 1558–1561, 2008.
17. Cao, X., Z. Q. Deng, G. Yang, et al., "Independent control of average torque and radial force in bearingless switched-reluctance motors with hybrid excitations," *IEEE Transactions on Power Electronics*, Vol. 24, No. 5, 1376–1385, 2009.
18. Lin, F.-C. and S.-M. Yang, "An approach to producing controlled radial force in a switched reluctance motor," *IEEE Transactions on Industrial Electronics*, Vol. 54, No. 4, 2137–2146, 2007.
19. Yang, Y., Z. Q. Deng, G. Yang, et al., "A control strategy for bearingless switched-reluctance motors," *IEEE Transactions on Power Electronics*, Vol. 25, No. 11, 2807–2819, 2010.
20. Afjei, E. and H. Torkaman, "The novel two phase field-assisted hybrid SRG: Magnetio static field analysis, simulation, and experimental confirmation," *Progress In Electromagnetics Research B*, Vol. 18, 25–42, 2009.

21. Torkaman, H. and E. Afjei, "Comprehensive magnetic field-based study on effects of static rotor eccentricity in switched reluctance motor parameters utilizing three-dimensional finite element," *Electromagnetics, Taylor and Francis*, Vol. 29, No. 5, 421–433, 2009.
22. Afjei, E. and H. Torkaman, "Finite element analysis of SRG under fault condition oriented towards diagnosis of eccentricity fault," *Applied Computational Electromagnetics Society Journal*, Vol. 26, No. 1, 8–16, 2011.
23. Afjei, E. and H. Torkaman, "Investigation of electromagnetic characteristics in external rotor SRM under dynamic eccentricity fault," *International Review of Electrical Engineering,* Vol. 6, No. 3, 1257–1263, 2011.
24. Torkaman, H. and E. Afjei, "Magnetostatic field analysis and diagnosis of mixed eccentricity fault in switched reluctance motor," *Electromagnetics, Taylor and Francis*, Vol. 31, No. 5, 368–383, 2011.
25. Torkaman, H. and E. Afjei, "Determining degrees of freedom for eccentricity fault in SRM based on nonlinear static torque function," *COMPEL: The International Journal for Computation and Mathematics in Electrical and Electronic Engineering*, Vol. 30, No. 2, 671–685, 2011.
26. Vaseghi, B., N. Takorabet, and F. Meibody-Tabar, "Transient finite element analysis of induction machines with stator winding turn fault," *Progress In Electromagnetics Research*, Vol. 95, 1–18, 2009.
27. Zhao, W., M. Cheng, R. Cao, et al., "Experimental comparison of remedial single-channel operations for redundant flux-switching permanent-magnet motor drive," *Progress In Electromagnetics Research*, Vol. 123, 189–204, 2012.
28. Lecointe, J. P., B. Cassoret, and J. F. Brudny, "Distinction of toothing and saturation effects on magnetic noise of induction motors," *Progress In Electromagnetics Research*, Vol. 112, 125–137, 2011.
29. Touati, S., R. Ibtiouen, O. Touhami, et al., "Experimental investigation and optimization of permanent magnet motor based on coupling boundary element method with permeances network," *Progress In Electromagnetics Research*, Vol. 111, 71–90, 2011.
30. Wang, Q. and X. Shi, "A an improved algorithm for matrix bandwidth and profile reduction in finite element analysis," *Progress In Electromagnetics Research Letters*, Vol. 9, 29–38, 2009.

31. Tai, C.-C. and Y.-L. Pan, "Finite element method simulation of photoinductive imaging for cracks," *Progress In Electromagnetics Research Letters*, Vol. 2, 53–61, 2008.
32. Mahmoudi, A., N. A. Rahim, and H. W. Ping, "Axial-flux permanent-magnet motor design for electric vehicle direct drive using sizing equation and finite element analysis," *Progress In Electromagnetics Research*, Vol. 122, 467–496, 2012.
33. Tian, J., Z.-Q. Lv, X.-W. Shi, et al., "An efficient approach for multifrontal algorithm to solve non-positive-definite finite element equations in electromagnetic problems," *Progress In Electromagnetics Research*, Vol. 95, 121–133, 2009.
34. Torkaman, H., N. Arbab, H. Karim, and E. Afjei, "Fundamental and magnetic force analysis of an external rotor switched reluctance motor," *Applied Computational Electromagnetics Society Journal*, Vol. 26, No. 10, 868–875, 2011.